



**HAL**  
open science

# A mathematical modeling of catalytic milli-fixed bed reactor for Fischer–Tropsch synthesis: Influence of tube diameter on Fischer Tropsch selectivity and thermal behavior

Giovanni Chabot, Richard Guilet, Patrick Cognet, Christophe Gourdon

## ► To cite this version:

Giovanni Chabot, Richard Guilet, Patrick Cognet, Christophe Gourdon. A mathematical modeling of catalytic milli-fixed bed reactor for Fischer–Tropsch synthesis: Influence of tube diameter on Fischer Tropsch selectivity and thermal behavior. *Chemical Engineering Science*, 2015, 127, pp.72-83. 10.1016/j.ces.2015.01.015 . hal-01917338

**HAL Id: hal-01917338**

**<https://hal.science/hal-01917338v1>**

Submitted on 9 Nov 2018

**HAL** is a multi-disciplinary open access archive for the deposit and dissemination of scientific research documents, whether they are published or not. The documents may come from teaching and research institutions in France or abroad, or from public or private research centers.

L'archive ouverte pluridisciplinaire **HAL**, est destinée au dépôt et à la diffusion de documents scientifiques de niveau recherche, publiés ou non, émanant des établissements d'enseignement et de recherche français ou étrangers, des laboratoires publics ou privés.



## Open Archive Toulouse Archive Ouverte

OATAO is an open access repository that collects the work of Toulouse researchers and makes it freely available over the web where possible

This is an author's version published in: <http://oatao.univ-toulouse.fr/20596>

### Official URL:

<https://doi.org/10.1016/j.ces.2015.01.015>

### To cite this version:

Chabot, Giovanni and Guilet, Richard and Cognet, Patrick and Gourdon, Christophe *A mathematical modeling of catalytic milli-fixed bed reactor for Fischer–Tropsch synthesis: Influence of tube diameter on Fischer Tropsch selectivity and thermal behavior.* (2015) *Chemical Engineering Science*, 127. 72-83. ISSN 0009-2509

Any correspondence concerning this service should be sent to the repository administrator: [tech-oatao@listes-diff.inp-toulouse.fr](mailto:tech-oatao@listes-diff.inp-toulouse.fr)

# A mathematical modeling of catalytic milli-fixed bed reactor for Fischer–Tropsch synthesis: Influence of tube diameter on Fischer Tropsch selectivity and thermal behavior

Giovanni Chabot <sup>a</sup>, Richard Guilet <sup>b,\*</sup>, Patrick Cognet <sup>a</sup>, Christophe Gourdon <sup>a</sup>

<sup>a</sup> Université de Toulouse, INPT, ENSIACET, Laboratoire de Génie Chimique (LGC UMR 5503), 4 Allée Emile Monso, F-31432 Toulouse, France

<sup>b</sup> Université de Toulouse, UPS, Laboratoire de Génie Chimique (LGC UMR 5503), 4 Allée Emile Monso, F-31432 Toulouse, France

## H I G H L I G H T S

- A two-dimensional pseudo-homogeneous model in packed bed reactors was built.
- Influence of tube reactor diameter for Fischer–Tropsch synthesis was investigated.
- Increasing tube diameter leads to hot spot within the reactor.
- Liquid hydrocarbons selectivity decreases if isothermal behavior is not fulfilled.
- High productivities in liquid hydrocarbons are obtained at millimeter scale.

## A B S T R A C T

A two-dimensional pseudo-homogeneous model has been developed to investigate the influence of tube size on the thermal behavior and performance of packed fixed bed reactor for the low temperature Fischer–Tropsch (FT) synthesis over alumina supported cobalt. Velocity, temperature and composition fields are determined by solving the fundamental transport equations in porous media. Special attention was paid to the variation of transport properties with temperature and composition of the gas mixture. High dependency of the thermal behavior on the thermal conductivity of the gas mixture is highlighted, whereas viscosity and heat capacity of gas mixture have very little influence. Moreover for the considered catalyst, simulation results have displayed high heat removal for the millimetric scale with a tube inner diameter below 2.75 mm for an extended range of weight hourly space velocity ( $20\text{--}600\text{ g}_{\text{syngas}}\text{ min}^{-1}\text{ kg}_{\text{cat}}^{-1}$ ,  $T=493\text{ K}$  and  $P=20\text{ bar}$ ). With a millimetric reactor, high CO conversion ( $X_{\text{CO}} > 90\%$ ) is obtained for values of space velocity between 30 and  $120\text{ g}_{\text{syngas}}\text{ min}^{-1}\text{ kg}_{\text{cat}}^{-1}$ . For higher diameter tube than 3.11 mm, thermal runaway occurs and even worse, no convergence achieved due to the very low heat transfer global coefficient and the weak surface/volume ratio, leading to a significant decrease of liquid fuels selectivity and an increase of light hydrocarbon ( $C_1$  to  $C_4$ ) selectivity up to 14%. To conclude, results from scale-up study with the millimetric scale are outstanding, more than  $2900\text{ kg h}^{-1}\text{ m}_{\text{cat}}^{-3}$  of  $C_{5+}$  could be produce after numbering-up 3033 tubes of 10 centimeters in length whereas conventional units (multitubular fixed bed reactors or slurry phase reactors) do not exceed  $400\text{ kg h}^{-1}\text{ m}_{\text{cat}}^{-3}$ .

### Keywords:

Fischer–Tropsch synthesis  
Fixed bed reactor  
Milli-reactor  
Intensification  
Reactor modeling  
COMSOL multiphysics

## 1. Introduction

Over the last few years, a major concern has arisen regarding the decreasing global oil reserves and the associated increasing crude oil price both driven by a strong world demand and by political

instabilities in oil producing regions. Thus, there is nowadays a strong need of alternative sources to supply the world demand for liquid fuels. For several years, first generation biofuels have been produced from the fermentation of sugars or starches to provide bioethanol for gasoline engine or else from the transesterification of vegetable oil to produce biodiesel. However this alternative to fossil fuels has become very controversial and is not indeed devoid of major drawbacks involving a new demand for lands that had been previously devoted to agricultural production and feeding people.

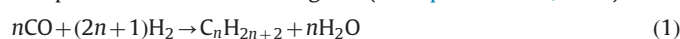
\* Corresponding author. Tel.: +33 5 34 32 37 18.

E-mail address: richard.guilet@iut-tlse3.fr (R. Guilet).

Nevertheless other agricultural feedstock like woodchips and residual of non-food parts of cereal crop, can be valorized and be integrated in a second-generation Biomass to Liquid process (BTL process) to synthesize liquid biofuels via the Fischer-Tropsch synthesis (FTS). This old process, which was developed in the 1920s, kindles a renewal of interest for providing a method to produce liquid hydrocarbons from synthesis gas, the so-called syngas, which is a mixture of CO and H<sub>2</sub>.

Historically the syngas was obtained from the gasification of coal (CTL process), but nowadays most of syngas is produced from the steam reforming or the partial oxidation of natural gas (GTL process). Moreover for a few years the gasification of biomass (BTL process) has been developed as a sustainable route. The former CTL and GTL processes are based on fossil resources whereas the latter technology BTL appears to be the most environmentally friendly technology owing to the great abundance of second-generation feedstocks which do not compete with the production of food crop.

More generally, the conversion of syngas via FT synthesis provides a wide product spectrum consisting of methane and a complex multi-component mixture predominantly of linear hydrocarbons (*n*-alkanes, *n*-alkenes) and oxygenates. Formation of paraffinic and olefinic compounds are respectively illustrated by the chemical equations (Eqs. (1) and (2)) whereas carbon dioxide is produced by the equilibrium reaction Water-Gas-Shift (Eq. (3)). Actually, the reaction mechanism featuring the chain growth follows a polymerization-like scheme based on sequential additions of the monomer CH<sub>2</sub>. The product range can be described by Anderson-Schultz-Flory (ASF) distribution, characterized by the chain growth probability parameter  $\alpha$  which can be considered as independent on the chain length *n* (Sadeqzadeh et al., 2012):



## 2. Background and objectives

### 2.1. Background

FT synthesis is known for its highly exothermicity ( $\Delta H_R = -165 \text{ kJ mol}_{\text{CO}}^{-1}$ ), therefore one of the most important concerns for the development of commercial FT reactors is their necessary heat removal capability that has a major impact on the products selectivity: a temperature increase has the effect of rising methane production as well as results in catalyst deactivation associated to sintering and coking. Four main types of commercial FT reactors are commonly implemented in industrial processes: the fluidized-bed reactor, the multitubular fixed-bed reactor (MFBR), the slurry phase reactor (SPR) and the circulating fluidized-bed reactor. Two operating processes have been developed: the high-temperature FT processes

(573–623 K, HTFT) and the low temperature FT processes (473–523 K, LTFT). HTFT based on iron catalysts yields essentially C<sub>1</sub>–C<sub>15</sub> hydrocarbons in circulating fluidized-bed reactors while LTFT processes lead mainly to linear long chain hydrocarbons (waxes and paraffins). Our study only deals with the LTFT processes for which two main technologies of reactor exist: the slurry-phase reactor and the multitubular fixed-bed reactor. Table 1, not intended to be exhaustive, gives the main advantages and drawbacks for both of them.

Although several drawbacks are identified, MFBR are widely used in FT process. These reactors are indeed capable of being easily scaled-up when going from a single tube to multitubular reactor to the extent that a good inlet distribution can be ensured. Moreover, many preliminary studies are carried out in packed-bed reactors at lab-scale such as catalyst developments, kinetic measurements and deactivation studies. Nevertheless, within years of development and improvement, some of these drawbacks have been reduced especially those regarding heat removal concerns. However, one of the main limitations of MFBR lies in high pressure drops that can arise when decreasing the catalyst particles diameter. No such limitation occurs in slurry phase reactors allowing consequently the use of particles as small as possible and higher effectiveness factors of the catalyst. Actually, particles diameters range from about 100  $\mu\text{m}$  when using a slurry reactor to about the millimeter for a MFBR. The use of smaller catalyst pellets in MFBR can obviously increase the effectiveness factor by reducing the diffusion limitations but the catalyst activity rises thereby and heat removal might be difficult to process using conventional reactors. Alternatively, the catalyst and/or the inlet reactor feed need to be highly diluted to prevent hot spot formation. On the other hand, process intensification that has emerged for the recent years has demonstrated the ability of new heat-exchanger reactors to operate in a new way with enhanced mass and heat transfers mainly due to a large surface to volume ratio. Actually, channel size mostly leads to laminar flow but the reduction of the diameter to millimeter allows avoiding unexpected transfer limitations. Milli-structured reactors allow for a strong increase of heat transport in radial direction and thus isothermal operation, even for highly exothermic reactions, becomes feasible.

Thus, recent works have shown that microchannel reactors and milli-fixed bed reactors were an alternative to conventional fixed-bed reactors, i.e. based on centimeter-scale tubes assembly, to operate FT synthesis. By greatly reducing the size and cost of chemical processing hardware, micro and/or milli-channel process technology holds the potential to enable cost effective production of synthetic fuels in smaller scale facilities. In particular, Velocys has developed a microchannel FT reactor. They announced a production from 28 to 40 barrels per day/full reactor with productivity several times higher than conventional process developed by Sasol or Shell. Cao et al. (2009) have performed experiments in microchannel reactor system with active cooling to maintain isothermal conditions in the catalyst bed. The catalytic portion of the reactor is a microchannel slot sandwiched within two separated oil-heating channels. Chambrey et al. (2011) experimentally compared with

**Table 1**  
Comparison between two commercial FT reactors operating the LTFT process (Dry, 2002).

	Advantages	Drawbacks
MFBR	Turbulent flow is ensured by the short distance between catalyst particles and especially by a high velocity of syngas Separation of liquid products from the catalyst phase is easy to process Plug flow conditions are obtained	High-pressure operation and pressure drop causes high gas compression costs Replacement of the catalyst requires special care Catalyst sintering can occur due to high operating temperature When tubes diameter increases, difficult heat removal and no temperature control can lead to hot-spot formation
SPR	Slurry phase is well mixed and tends to isothermal conditions High productivity per mass of catalyst (lower charge than for fixed bed reactor)	Separation of the wax product from the catalyst is difficult Well mixed reactor behavior tends to decrease the reactions rates

centimetric and millimetric tubular fixed bed reactors under exactly the same operating conditions (CoPt/Al<sub>2</sub>O<sub>3</sub>, 220 °C, 20 bar, H<sub>2</sub>/CO<sub>2</sub>). The authors found an increase from 40 to 60% of conversion indicating that the millimetric fixed bed represented a real gain in term of productivity. The reasons of this improvement are unclear: absence of internal temperature gradient, role of the hydrodynamics of both phases as the expected increase of the superficial velocity for smaller reactor diameter. Many other works report and highlight the interest in producing biofuels in intensified reactors. [Knochen et al. \(2010\)](#) concluded that a milli-structured fixed-bed reactor was an interesting option for small FTS plants since high volume specific productivity can be obtained at acceptable pressure drops. Moreover, [Myrstad et al. \(2009\)](#) showed the ability of structured reactor to operate FT synthesis with high active catalyst at severe conditions without thermal runaway and subsequent high deactivation of the catalyst. Catalyst grafted on stainless steel walls of a microchannel reactor substrate demonstrated high activity under FT reaction. Activity and selectivity were higher under microchannel conditions than in a classical fixed-bed catalytic reactor ([Guillou, 2005](#)). In addition to these experimental studies, some works based on numerical simulations ([Atwood and Bennett, 1979](#); [Bub et al., 1980](#); [Jess et al., 1999](#); [Wang et al., 2003](#); [Wu et al., 2010](#)) have concluded that FT synthesis carried out in intensified systems is enhanced considerably due to mass and heat transfer increase. Actually a few mathematical modeling studies on fixed bed FT reactors have been reported in literature. An oversimplified 1-D heterogeneous plug flow model was used to describe a centimetric reactor as early as 1979 ([Atwood and Bennett, 1979](#)). Although intraparticle diffusion was considered with the assumption that the kinetics was first order in CO, no model of product distribution was developed. Now, several FT reactors 1-D or 2-D models have been developed based on various assumptions. A comparison between one-dimensional and two-dimensional model suggested that the 2-D model leads to more accurate prediction when thermal runaway occurs ([Jess and Kern, 2009](#)). Some authors ([Jess and Kern, 2009, 2012](#); [Lee and Chung, 2012](#)) reported that hot spots and radial temperature gradients occurred using a 4.6-centimeter tube diameter with particle diameter close to 3 mm. Although numerous parameters were studied in these works such as inlet temperature, cooling temperature, particle diameter or molar ratio H<sub>2</sub>/CO, no parametric study concerning the tube diameter has been performed in the millimetric range.

## 2.2. Objectives

The main objective of this work is to study how the diameter affects the reactor behavior in terms of conversion, selectivities, temperature gradients and production of the various hydrocarbon fractions. The model system is based on double-shell packed-bed reactor with various diameter. A computational 2-D model coupled with mass and heat transport and hydrodynamic equations is used to predict how the FT reaction occurs. The hot-spot formation and pressure drop within the reactor were investigated according to the diameter with regards to parameters such as weight hourly space velocity (WHSV) and shell cooling temperature. Finally, the potential of milli-structured is evaluated in a short scale-up study.

## 3. Kinetics of Fischer–Tropsch synthesis

The major challenge in kinetic modeling is to describe the FT reaction with regards to the complexity of the reactions mechanisms and the large number of species involved. Some models are based only on CO and/or H<sub>2</sub> conversion and do not consider the selectivity although those are both greatly influenced by temperature gradients. According to [Lee and Chung \(2012\)](#), three different

approaches to describe FT kinetics arise: (1) kinetic model based on mechanistic proposal consisting in a sequence of elementary reactions involving adsorbents and/or intermediates; (2) empirical expressions of general power-law kinetics; and (3) semi-empirical kinetics based on FT mechanisms. The third approach is generally based on Langmuir–Hinselwood–Hougen–Watson (LHHW) model equations. On the basis of carbide or enolic mechanisms, [Sarup and Wojciechowski \(1989\)](#) defined with regards to LHHW equations a kinetic model for the FT synthesis rate regarding CO and H<sub>2</sub>, consumption which the general form is given by

$$r_{FT} = \frac{k_{FT} P_{CO}^a P_{H_2}^b}{\left(1 + \sum_i k_i P_{CO}^{c_i} P_{H_2}^{d_i}\right)^2} \quad (4)$$

A review of kinetics equation for iron-based catalyst is given by [Huff and Satterfield \(1984\)](#) and [Zimmerman and Bukur \(1990\)](#). Many investigators also worked on kinetics expression for cobalt-based catalyst ([Anderson et al., 1951](#); [Outi et al., 1981](#); [Sarup and Wojciechowski, 1989](#); [Yates and Satterfield, 1991](#)). The latter simplified the equations of Sarup and Wojciechowski down to only two parameters: the reaction constant  $k_{FT}$  and the adsorption constant  $k_1$ :

$$r_{FT} = \frac{k_{FT} C_{CO} C_{H_2}}{(1 + k_1 C_{CO})^2} \quad (5)$$

Regarding the catalyst, iron and cobalt on various oxide supports have been widely used for FT synthesis. A short description of their respective advantages and drawbacks is given by [Khodakov et al. \(2007\)](#). Although cobalt catalysts are more expensive than iron ones, cobalt catalysts exhibit a greater resistance to attrition, a higher productivity and a lower sensitivity to water. Moreover, a product distribution model has been developed by [Philippe et al. \(2009\)](#) at high temperature over cobalt-based catalyst. Only paraffin production according to Eq. (1) is considered. Indeed, for sake of simplicity in the modeling, olefins (Eq. (2)) and oxygenates productions are not examined and the formation of carbon dioxide by Water Gas Shift reaction (Eq. (3)) is neglected, cause of the weak activity of cobalt based catalyst for the WGS reaction ([Newsome, 1980](#)). All kinetic parameters and adsorption constant  $k_1$  follow Arrhenius law and activation energies are taken from [Philippe et al. \(2009\)](#). The monoxide carbon consumption rate is

$$r_{CO} = -r_{FT} \quad (6)$$

with

$$r_{FT} = \frac{a \cdot \exp\left(\frac{-E_a}{RT}\right) \cdot C_{CO} \cdot C_{H_2}}{\left(1 + b \cdot \exp\left(\frac{-\Delta H_b}{RT}\right) \cdot C_{CO}\right)^2} \quad (7)$$

From the stoichiometry of Eq. (1), water formation rate becomes

$$r_{H_2O} = -r_{CO} = +r_{FT} \quad (8)$$

Production rates of methane  $r_{C_1}$  and ethane  $r_{C_2}$  are written following two specific laws with two temperature dependent parameters via Arrhenius law:

$$r_{C_1} = d \cdot \exp\left(\frac{-E_d}{RT}\right) \cdot r_{FT} \quad (9)$$

$$r_{C_2} = e \cdot \exp\left(\frac{-E_e}{RT}\right) \cdot r_{FT} \quad (10)$$

For higher linear hydrocarbons ( $n > 2$ ) each hydrocarbon production rate is determined using a recursive kinetic model based on Anderson–Schultz–Flory theory. A constant chain growth probability ( $\alpha=0.9$ ) is used. Thus, hydrocarbons production rate was given as

$$r_{C_n} = \alpha \cdot r_{C_{n-1}} \quad (11)$$

Moreover, the stoichiometry of reaction (1) leads to the consumption rate of hydrogen as follows:

$$-r_{H_2} = \sum_i^N (2i+1) \cdot r_{C_i} \quad (12)$$

And also

$$-r_{CO} = 1 \cdot r_{C_1} + 2 \cdot r_{C_2} + 3 \cdot r_{C_3} + \dots + N \cdot r_{C_N} = \sum_{i=1}^N i \cdot r_{C_i} \quad (13)$$

Therefore the consumption of hydrogen can be expressed:

$$-r_{H_2} = 2 \cdot r_{CO} + \sum_{i=1}^N r_{C_i} \quad (14)$$

Kinetics parameters and activation energy used in the current study are listed in Table 2 and were taken from Sadeqzadeh et al. (2012) at steady state. In this study, hydrocarbon chains were assumed to grow up to not more than 50.

#### 4. Mathematical modeling of packed bed reactor

A 2D axisymmetric geometry was built and a fully-coupled physics model with concentrated medium mass transport, heat transfer in fluids and Brinkman equations for the velocity profile and continuity equation are used to simulate transports phenomena and formations of hydrocarbons. A mixture of CO and H<sub>2</sub> enters the packed-bed reactor with a mass flow,  $F$ , an inlet temperature,  $T_0$  and a hydrogen to carbon monoxide molar ratio,  $\theta_{H_2/CO}$ . A double-shell ensures the cooling and/or heating of the system where a thermal fluid flows all around the external reactor tube (Fig. 1). The hydrocarbon products are mainly under gas phase but formed liquid waxes go through the reactor down to the outlet. Thus, the flow through the porous medium, i.e. the catalytic packed bed of solid particles, is a two-phase flow with an increasing liquid flow as the hydrocarbons chains grow.

Some assumptions were made to undertake the modeling of the reactor. As far as possible the relevance of these assumptions is studied in this paper.

1. Under the operating conditions, liquid phase flow was neglected (Philippe et al., 2009), so that a pseudo-homogeneous model

was chosen where gas and solid were only considered. Waxes formation was not included in the hydrodynamic model.

2. A laminar flow occurs and Reynolds number was calculated from spherical pellets mean diameter.
3. The effective diffusion of gaseous reactant through the liquid-filled phase pores of the catalyst was not considered as a limitation so that intraparticle mass transport particle limitation was neglected. Thus, effectiveness factor was considered to be close to one.
4. The production of oxygenates and WGS reactions were neglected due to their low occurrence when using FT synthesis cobalt-based catalyst.
5. All gas streams were supposed to be ideal, thus the ideal gas law was applied to evaluate the density of gas phase and concentration of gases species.
6. The tubular packed-bed reactor runs at steady state.
7. The bed porosity was assumed to be constant throughout the packing of the bed.

Physical properties of gas stream were considered as function of temperature, pressure and composition. The viscosities  $\mu_{g,i}$ , thermal conductivities  $\lambda_{g,i}$ , specific heat capacities  $c_{p,i}$  and enthalpies of formation of hydrocarbons  $\Delta H_{f,i}$  of pure gas compounds were estimated by polynomial expressions given by Yaws (1999). The viscosity of gas mixtures  $\mu_{g,m}$  was calculated using Wilke's method as described by Poling et al. (2000) with the modification of Brokaw (1969). Regarding thermal conductivity of gas mixtures  $\lambda_{g,m}$  the Wassiljewa equation (Poling et al., 2000) with Brokaw's approach (Brokaw, 1969) was used.

The physical catalyst properties, 25%Co/0.1% Pt/Al<sub>2</sub>O<sub>3</sub>, are associated to the chosen kinetic model described above in Section 3. The main characteristics taken from Sadeqzadeh et al. (2012) are summarized in Table 3.

**Table 3**  
Characteristics of the catalyst CoPt/Al<sub>2</sub>O<sub>3</sub> used by Sadeqzadeh et al. (2012).

Particle diameter, $d_p$ ( $\mu\text{m}$ )	Density, $\rho_{cat}$ ( $\text{kg m}^{-3}$ )	Cobalt content (%)	Void fraction of bed $\epsilon$ (-)
90	2030	25	0.4

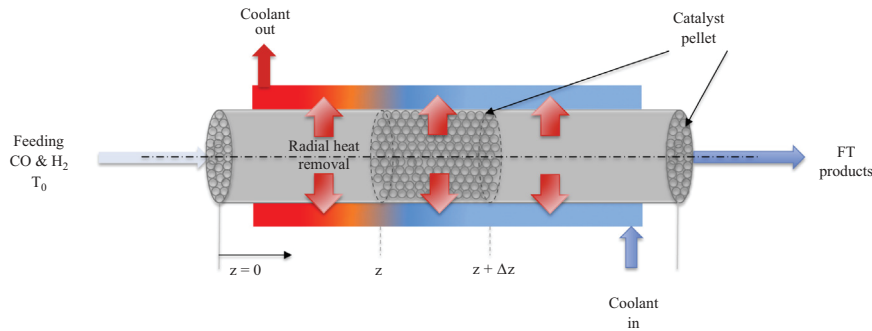


**Fig. 1.** Schematic axisymmetric tubular packed bed FT reactor.

**Table 2**  
List of kinetic parameters used in this study (Sadeqzadeh et al., 2012).

$a^a$ ( $\text{m}^6 \text{kg}_{cat}^{-1} \text{mol}^{-1} \text{s}^{-1}$ )	$E_a$ ( $\text{kJ mol}^{-1}$ )	$b^a$ ( $\text{m}^3 \text{mol}^{-1}$ )	$\Delta H_b$ ( $\text{kJ mol}^{-1}$ )	$d^a$ (-)	$E_d$ ( $\text{kJ mol}^{-1}$ )	$e^a$ (-)	$E_e$ ( $\text{kJ mol}^{-1}$ )	$\alpha$ (-)
$7.17 \times 10^7$	100	44.93	20	$3.80 \times 10^7$	81	$2.01 \times 10^3$	49	0.9

<sup>a</sup> a, b, d and e are the pre-exponential factors in the Arrhenius laws.

#### 4.1. Momentum and continuity equations

In order to describe flow in porous media and compute fluid velocity profile, the Brinkman equation (Eq. (15)), derived form of Navier–Stokes equation in porous media, was adopted. Considering the above mechanism (Eq. (1)), the total conversion of CO towards  $n$ -alkane  $C_n$  involves the consumption of  $2n$  moles of gas compound in the total molar flux. Thus, the FT synthesis leads to a decreasing of the volumetric gas flowrate, which also modifies the density, thus a compressible flow formulation of the continuity equation (Eq. (16)) was used with the steady-state approximation coupled with the Brinkman equation:

$$\nabla \cdot \left[ -p\mathbf{I} + \frac{\mu_{g,m}}{\epsilon} \nabla \vec{u} \right] - \frac{\mu_{g,m}}{K} \vec{u} - \beta_F \|\vec{u}\| \vec{u} = \vec{0} \quad (15)$$

$$\nabla \cdot (\rho_{m,f} \vec{u}) = 0 \quad (16)$$

Considering a laminar flow regime ( $Re_p < 1$  Nield and Bejan, 2013) with very low velocity, even if laminar flow though packed bed is fulfilled for  $Re_p/(1-\epsilon) < 10$ , the Brinkman viscous terms are predominant compared to the inertial term represented by the quadratic velocity term (Chukwudozie et al., 2012; Marpu, 1995). The porous media permeability  $K$  was determined using Carman–Kozeny:

$$K = \frac{\epsilon^3}{180(1-\epsilon)^2 d_p^2} \quad (17)$$

#### 4.2. Transport species equations

The local mass balance at steady state for each species  $i$  was given by Eq. (18). Axial and radial dispersion, convection and source terms were considered:

$$\nabla \cdot \vec{j}_i + \rho_{m,f} (\vec{u} \cdot \nabla) w_i = \rho_{cat} M_i (1-\epsilon) \eta r_i \quad (18)$$

The mass flux density of specie  $i$ , noted  $\vec{j}_i$ , caused by axial and radial dispersion is modelled by a Fick's law analogy:

$$\vec{j}_i = -\rho_{m,f} D_e \nabla w_i \quad (19)$$

where  $D_e$  is a diagonal matrix lumping the effective axial  $D_{ea}$  and radial  $D_{er}$  dispersion coefficient. For low value of the Reynolds number ( $Re_p \leq 1$ ) which is our case, the two dispersion coefficients are approximately the same (Delgado, 2006) and also equal to the average molecular diffusion coefficient  $D_i^m$  (Eq. (20)) (Delgado, 2006) calculated from binary diffusion constant  $D_{i,j}$ .

$$D_i^m = \frac{1-w_i}{\sum_{k \neq i} \frac{X_k}{D_{i,k}}} \quad (20)$$

The diffusion coefficients for binary gas systems  $D_{i,j}$  were estimated with empirical correlations proposed by Fuller and Giddings (1965), Fuller et al. (1966, 1969). The local mass balance for each compound in the gas phase was rewritten according to

$$\rho_{m,f} (\vec{u} \cdot \nabla) w_i - \vec{\nabla} \cdot (\rho_{m,f} D_i^m \nabla w_i) = \rho_{cat} M_i (1-\epsilon) \eta r_i \quad (21)$$

The kinetic model developed above gave the source terms corresponding to the intrinsic rate of formation for each compound. The effectiveness factor was calculated as the ratio between effective CO consumption and the consumption at the pellet surface.

$$\eta = \frac{r_{CO}^{effective}}{r_{CO}^{surface}} \quad (22)$$

The investigation of competition between pore diffusion and reaction is only based on CO consumption rate due to recursive kinetics of hydrocarbons forming reactions. Therefore a pseudo-

first-order rate was written for the consumption rate of carbon monoxide assuming a low conversion of CO:

$$-r_{CO} = k'_a C_{H_{2g}} \quad (23)$$

with

$$k'_a = k_a \frac{C_{CO_g}}{(1+k_b C_{CO_g})^2} \quad (24)$$

The effectiveness factor is also defined as function of Thiele modulus  $\phi$ :

$$\eta = \frac{\tanh \phi}{\phi} \quad (25)$$

where the Thiele's modulus  $\phi$  was modified so as to take into consideration hydrogen diffusion through the pore, filled with liquid wax, inside the pellet:

$$\phi = \frac{d_p}{6} \sqrt{\frac{\rho_{cat} k'_a C_{H_{2g}}}{D_{eff,H_2,l} C_{H_{2l}}}} \quad (26)$$

The Henry's law gave value of hydrogen concentration in liquid wax:

$$C_{H_{2l}} = \frac{P_{H_2}}{H_{e_{H_2}}} = \frac{RT}{H_{e_{H_2}}} C_{H_{2g}} \quad (27)$$

Only a fraction of porous media is permeable to dissolved hydrogen and the path of diffusion through the porous particles filled with liquid hydrocarbons, is random and tortuous (Table 4). Thus, to estimate effective diffusion coefficient of dissolved hydrogen through the catalyst pores, the tortuosity ( $\tau_p$ ) and the porosity ( $\epsilon_p$ ) of particle were taken into account in the estimation:

$$D_{eff,H_2,l} = \frac{\epsilon_p}{\tau_p} D_{m,H_2,l} \quad (28)$$

#### 4.3. Heat transport

In a 2D axial and radial dispersion plug flow model, heat transport is ensured by convection and thermal dispersion. The fluid and the solid were assimilated to a homogeneous body – the bed – though heat is transferred by either axial or/and radial thermal dispersion. Radiative transport is neglected in our case. Based on the same assumptions for transport species, the heat balance was written as

$$\rho_{m,f} c_{p,g,m} \vec{u} \cdot \nabla T = \nabla \cdot (\lambda_e \nabla T) + \sum_{i=1}^N \Delta H_{f,i} r_i \rho_{cat} (1-\epsilon) \quad (29)$$

Several theoretical and experimental studies have been performed on the determination of the effective thermal conductivity  $\lambda_e$  which is a matrix lumping the radial thermal conductivity  $\lambda_{er}$  and the axial thermal conductivity  $\lambda_{ea}$  (Özgümüş et al., 2013). Predictive correlations for the axial or the radial thermal conductivity  $\lambda_{ei}/\lambda_{g,m}$  (the subscript  $i$  refers to  $a$  for axial or  $r$  for radial thermal conductivity) are mainly expressed in a linear form with respect to particle based Reynold ( $Re_p$ ) or Peclet number ( $Pe_p = Re_p Pr$ ) such as the following equation:

$$\frac{\lambda_{ei}}{\lambda_{g,m}} = \frac{\lambda_{bed}}{\lambda_{g,m}} + K Re_p Pr \quad (30)$$

**Table 4**  
Parameters used for the Thiele modulus evaluation.

$He_{H_2}$ (Pa m <sup>3</sup> mol <sup>-1</sup> )	$D_{m,H_2,l}$ (m <sup>2</sup> s <sup>-1</sup> )	$\epsilon_p/\tau_p$ (-)
20,000	$4.0 \times 10^{-8}$	0.3

The value for the radial effective heat conductivity  $\lambda_{er}$  can be well described by the correlation of [Bauer and Schlunder \(1978a,b\)](#):

$$\frac{\lambda_{er}}{\lambda_{g,m}} = \frac{\lambda_{bed}}{\lambda_{g,m}} + \frac{Re_p Pr}{7 \left[ 2 - (1 - 2d_p/d_R)^2 \right]} \quad (31)$$

with  $\lambda_{bed}$  the effective thermal conductivity when no fluid flows, which is in fact the static contribution of the effective thermal conductivity. Thus, the ratio  $\lambda_{bed}/\lambda_{g,m}$  is constant and is usually in the range 2–10. As suggested by [Jess and Kern \(2012\)](#) the ratio was taken equal to 4 according to [Borkink and Westerterp \(1992\)](#). Axial effective heat coefficient  $\lambda_{ea}$  was calculated by the following correlation ([Springer, 2010](#)):

$$\frac{\lambda_{ea}}{\lambda_{g,m}} = \frac{\lambda_{bed}}{\lambda_{g,m}} + \frac{Re_p Pr}{2} \quad (32)$$

#### 4.4. Boundary conditions

The flow in the reactor is driven by pressure drop, so that the outlet pressure is equal to the constant value  $P_{out}$ . No slip condition is applied, thus the velocity  $u_{wall}$  in the wall vicinity tends to zero.

Following boundary conditions were applied at inlet and outlet:

$$\text{At } r = 0 : \vec{u}(r, 0) = \vec{u}_0 \quad (33)$$

$$T(r, 0) = T_0 \quad (34)$$

$$w_i(r, 0) = w_{i,0} \quad (35)$$

$$P(r, L) = P_{out} \quad (36)$$

Symmetric boundary conditions are

$$\forall z, r = 0 : \frac{\partial w_i}{\partial r} = \frac{\partial T}{\partial r} = 0 \quad (37)$$

Wall boundary conditions are

$$\forall z, r = R : \vec{u}(R, z) = \vec{0} \quad (38)$$

$$\frac{\partial w_i}{\partial r} = 0 \quad (39)$$

$$\lambda_{er} \frac{\partial T}{\partial r} = U_{overall} \times (T - T_w) \quad (40)$$

with

$$\frac{1}{U_{overall}} = \frac{d_R}{8\lambda_{er}} + \frac{1}{\alpha_{w,int}} + \frac{e}{\lambda_{wall}} + \frac{1}{\alpha_{w,ext}} \quad (41)$$

The term  $U_{overall}$  represents the overall thermal transmittance in the vicinity of the wall. The wall heat transfer coefficient  $\alpha_{w,int}$  is calculated from the following correlation of [Martin and Nilles \(1993\)](#):

$$Nu_w = \frac{\alpha_{w,int} d_p}{\lambda_{g,m}} = \left( 1.3 + 5 \frac{d_p}{d_R} \right) \frac{\lambda_{bed}}{\lambda_{g,m}} + 0.19 Re_p^{3/4} Pr^{1/3} \quad (42)$$

Heat transfer by pure diffusion through the wall was neglected by considering the thin material thickness and the high thermal conductivity of the stainless steel wall. The external heat transfer limitation was also neglected by assuming high velocity of the cooling fluid in the shell. Thus, boundary condition (Eq. (40)) at the wall cooling was rewritten as

$$\forall z, r = R : \lambda_{er} \frac{\partial T}{\partial r} = \alpha_{w,int} \times (T - T_w) \quad (43)$$

The global heat released by the Fischer–Tropsch synthesis was computed from the enthalpy of formation ([Yaws, 1999](#)) of each hydrocarbon depending on bulk temperature.

#### 4.5. Computational methods

Commercial CFD software COMSOL Multiphysics version 4.3b installed on a workstation with Intel Xeon 8 cores at 2.66 Ghz with 16 GB RAM was used to solve the coupled equations for the modeling of the FT packed bed reactor. A free triangular mesh depending on the tube diameter is used. Given the constant number of dependent variables, degrees of freedom (DOFs) only depends of the grid fineness or the number of nodes. Values of DOFs were about 250,000 depending on tube diameter. A grid refinement was also performed in the vicinity of the inlet of the reactor where hot spot potentially occurs to ensure reasonable accuracy of solutions. Parameters used for the simulation are summarized in [Table 5](#).

Transport properties such as dynamic viscosity, thermal conductivity and specific heat of gases were evaluated as function of the bulk gas phase composition and temperature by using external MATLAB function. Simulations were carried out in order to examine the variations of the transport properties. All transport properties change along the reactor due to changes in composition and temperature of gas stream. Nevertheless, heat capacity and viscosity variations do not exceed 30% of the inlet value whereas thermal conductivity decreases of a factor of 3.4. Thus, other simulations were carried out using constant transport properties. Only thermal conductivity ( $\lambda_{g,m}$ ) exhibited a significant impact on the thermal behavior of milli-fixed bed reactor. Indeed simulation, where thermal conductivity was kept to be constant ( $\lambda_{g,m} = 0.134 \text{ W m}^{-1} \text{ K}^{-1}$ ,  $\theta_{H_2/CO} = 2$ ,  $T_w = 493.15 \text{ K}$ ), led to a difference of more than 20 K on the maximal temperature reached within the bed. This maximum varies from 503.4 K when the thermal conductivity is kept constant to 524.5 K when it is not. Other simulations have highlighted a variation of less than 1 K between the cases when heat capacity and viscosity of gases mixture are kept constant or not along the reactor. Thus, in this study, the viscosity and the heat capacity of gas mixture were kept constant, calculated at the inlet conditions, whereas the change in thermal conductivity was considered in order to achieve a satisfactory degree of accuracy in the model output.

## 5. Results and discussion

### 5.1. Intraparticle concentration profile

It is of interest to investigate the interaction between diffusion and reaction in a Fischer–Tropsch catalyst pellet. The mathematical model previously introduced was based on effectiveness factor defined as Eq. (22). A strong dependence of the effectiveness factor was found

**Table 5**

Data and operating conditions used to model the packed fixed bed reactor for Fischer Tropsch synthesis.

Parameters	Value
$P_{out}$	20 bar
$T_0$	293.15 K
WHSV	20–600 $\text{g}_{\text{syngas}} \text{ min}^{-1} \text{ kg}_{\text{cat}}^{-1}$
$\theta_{H_2/CO}$	2 (-)
$\alpha$	0.9 (-)
$e$	0.4 (-)
$T_w$	488.15–503.15 K
$\mu_{g,m}^a$	$2.4 \times 10^{-5} \text{ Pa s}$
$\lambda_{g,H_2}^a$	$250 \text{ W m}^{-1} \text{ K}^{-1}$
$\lambda_{g,CO}^a$	$0.0376 \text{ W m}^{-1} \text{ K}^{-1}$
$\lambda_{g,m}^a$	$0.134 \text{ W m}^{-1} \text{ K}^{-1}$

<sup>a</sup> Estimated values for the inlet at  $T = 493.15 \text{ K}$  and molar ratio  $\theta_{H_2/CO} = 2$  for mixture.

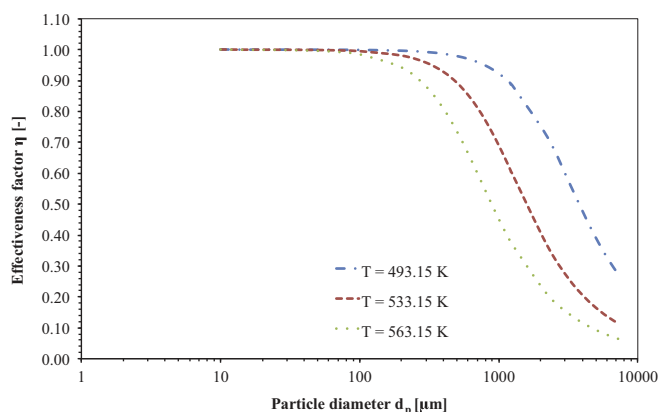


**Fig. 2.** Variation of effectiveness factor with pellet size for three different temperatures.

**Table 6**

Volume and molar fraction of compounds under FT operating conditions,  $d_R = 1.75$  mm,  $WHSV = 70$  g<sub>syngas</sub> min<sup>-1</sup> kg<sub>cat.</sub><sup>-1</sup>.

Compounds	Phase	Production (493.15 K, 20 bar) $P_V$ (L h <sup>-1</sup> kg <sub>cat.</sub> <sup>-1</sup> )	Volume fraction (%)	Molar fraction (%)
H <sub>2</sub> O	Gas	401.64	88.95	86.85
H <sub>2</sub>	Gas	2.08	0.46	0.45
CO	Gas	20.01	4.43	4.33
C <sub>1</sub> -C <sub>6</sub>	Gas	26.02	5.76	5.63
C <sub>7</sub> -C <sub>50</sub>	Liquid	1.77	0.39	2.74

according to the pellet size (Fig. 2) whatever the operating temperature. However it can be seen that, for very small catalyst particle ( $d_p = 90$ – $100$   $\mu\text{m}$ ), the CO-based effectiveness factor is close to one. With increasing the particle diameter size and/or boosting the operating temperature, the effectiveness factor decreases to a relatively low value involving severe limitation of diffusion inside the pores. Moreover, the results show that, for pellets size of about 2–4 mm, the diffusion within the catalyst pore cannot be neglected. Thus, the assumption that the effectiveness factor is equal to one is verified as far as in the present model the catalyst particle diameter is 90  $\mu\text{m}$ .

### 5.2. Gas–liquid hydrocarbon phase ratio under typical operating conditions

As indicated previously, reactor simulation was chosen to be carried out by solving the species transport equations and the Brinkman equations for gaseous compounds only ( $T_w = 493.15$  K and  $P_{out} = 20$  bar). Indeed under these operating conditions, thermodynamics equilibrium calculations (National Institute of Standards and Technology (NIST), 2013) revealed that hydrocarbons from C<sub>1</sub> to C<sub>6</sub> were in gaseous phase whereas compounds from C<sub>7</sub> to C<sub>50</sub> were in liquid phase. Simulation results reveal that the pseudo homogeneous model is relevant regarding gaseous versus liquid flow ratio (Table 6). ASF distribution was used to describe hydrocarbons production over C<sub>6</sub> and results highlight that 99% of the volumetric flow representing more than 96% molar of total compounds are in the gas phase.

### 5.3. Influence of tube diameter on temperature profile and selectivity at constant WHSV

The effect in changing the tube diameter toward millimetric scale with regard to the behavior of the reactor is investigated. The first purpose was to carry out the study according to eight diameters of millimetric to centrimetric size using standard stainless steel tube

diameters, i.e. 1", 3/4", 5/8", 1/2", 3/8", 1/4", 1/8" and 1/16" with standard thicknesses. The first results in temperature contours and hot spot formation showed that no convergence was achieved for tube diameters higher than 1/4" (6.35 mm). Actually for those diameters, temperature within the catalytic bed increases drastically with no possible control of the reaction heat release and the thermal runaway leads to undefined solutions of the simulation. This was observed whatever the chosen WHSV. Actually, this is explained by the activity of the catalyst associated to high effectiveness factor ( $\eta$ ). Thus, the results reported here focus on diameters ranging from 0.88 mm to 3.11 mm as internal diameter ( $d_R$ ). It was decided to investigate the influence of the diameter without any dilution of the catalyst that would have allowed the use of large tubes.

Space velocity ( $WHSV = 20$  g<sub>syngas</sub> min<sup>-1</sup> kg<sub>cat.</sub><sup>-1</sup>), cooling temperature ( $T_w = 493.15$  K and molar ratio hydrogen to carbon monoxide ( $\theta_{H_2/CO} = 2$ ) were chosen as constant parameters. The two-dimensional temperature contours are depicted for two different tubes diameters (Fig. 3). Fig. 3 highlights the formation of hot spots as the tube diameter increases. For the lowest given diameter, i.e. 0.88 mm (Fig. 3a), isothermal contour arises (in yellow color) and the maximum reached temperature does not exceed 494.3 K. As the diameter rises, maximum temperature increases up to 621.4 K, i.e. temperature changes from yellow to red in color (Fig. 3b), hot spot appears and gets closer to inlet of the reactor. In all cases near the inlet region, the flow is heated up by the heat transfer fluid. Indeed heat transport by diffusion (black arrows) operates from the wall, that is a hot region near the inlet, towards the centerline and the coolest regions. Particularly when the hot spot arises, the heat is removed by the coolant fluid outside of the packed bed. In the vicinity of the hottest zone a part of the heat released is transported by thermal diffusion boosting the temperature increases of the reactor bulk flow in the coolest zone. For this reason the diffusive heat flux is substantially opposed to the convective heat flux (red arrows).

The axial temperature profile is illustrated in Fig. 4 for different pipe sizes reported in metric value.

It can be observed that better heat removal and a flat temperature profile within the bed can be obtained with lowest tube diameter. Between 0.88 mm and 2.00 mm inner tube diameter, the system removes efficiently the heat released during the synthesis; no thermal runaway is observed within the bed. Only a slight increase up to 6 K over the cooling temperature ( $T_w$ ) is observed when the diameters reaches 2.00 mm. Above 3.10 mm and as mentioned previously, thermal runaway occurs and temperature increasing is so drastic that no convergence of the simulation is possible. The thermal behavior reported in Fig. 4 is in agreement with the two-dimensional centimeter models developed by Jess and Kern (2012) and Lee and Chung (2012) in centimeter tubes. They showed how the performance of the reactor and the maximal temperature reached are highly sensitive with tube diameters and catalyst particle size.

The maximal temperature  $T_{max}$  within the bulk is correlated to the tube diameter of the FT reactor (Fig. 5). As shown in Fig. 5, space velocities in the range of 20–80 g<sub>syngas</sub> min<sup>-1</sup> kg<sub>cat.</sub><sup>-1</sup> seems to have no effect on the maximal temperature. As the diameter decreases, the maximal temperature induced by the heat released by the FT synthesis decreases towards the setpoint temperature  $T_w$ . Actually, for the studied diameters, the CO conversion does not change significantly in the given conditions of WHSV as the residence time is high enough. So, the total heat released rises with WHSV due to the total gas flow increasing. For smaller diameters, overall heat transfer coefficients are so high that no difference in  $T_{max}$  is observed as WHSV increases. At a given WHSV, with increasing tube diameter, the heat removal from the core to the wall cooling decreases. Indeed when diameter increases, overall heat transfer coefficient gets lower and the ability of the reactor to remove reaction heat diminishes.

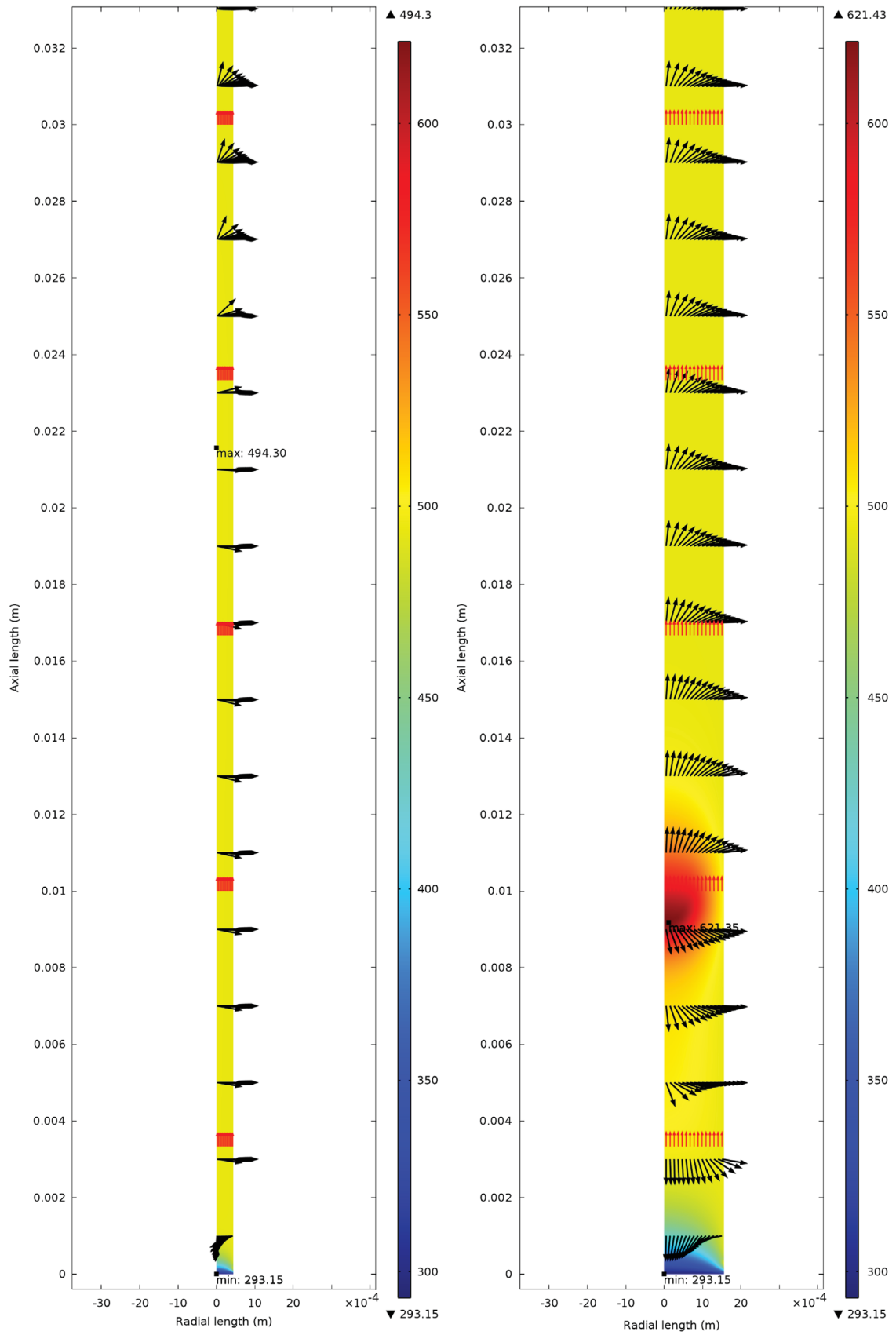


**Fig. 3.** Temperature contours, diffusive heat flux (black arrow) and convective heat flux (red arrow) within the fixed bed reactor under operating condition  $T_w = 493.15$  K,  $WHSV = 20 \text{ g}_{\text{syngas}} \text{ min}^{-1} \text{ kg}_{\text{cat}}^{-1}$  for different tube diameters. (For interpretation of the references to color in this figure caption, the reader is referred to the web version of this article.)

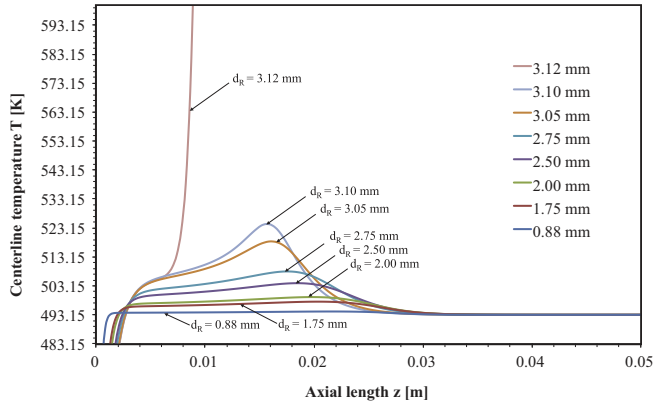


Fig. 4. Influence of the tube diameter on the temperature ( $r=0$ ) along axial direction of a cooled tubular fixed bed reactor ( $WHSV = 20 \text{ g}_{\text{syngas}} \text{ min}^{-1} \text{ kg}_{\text{cat}}^{-1}$ ).

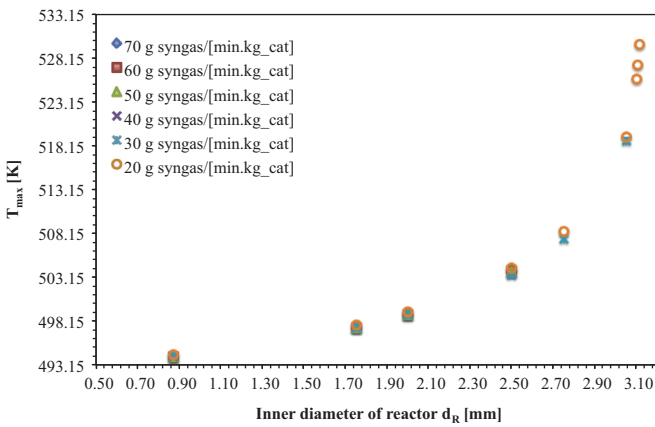


Fig. 5. Maximal temperature versus tube diameter for different space velocity ( $T_w = 493.15 \text{ K}$ ).

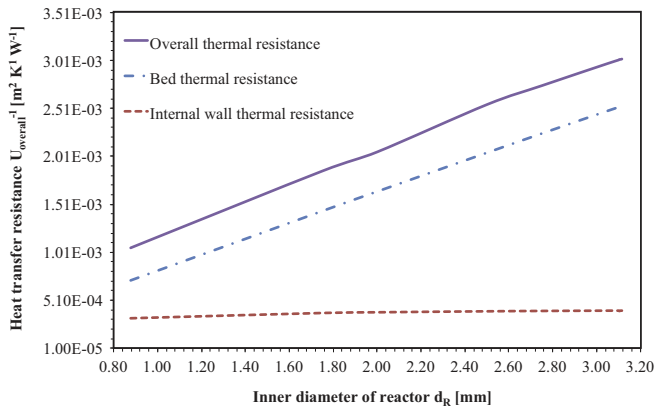


Fig. 6. Heat transfer resistance versus tube diameter reactor ( $T_w = 493.15 \text{ K}$ ,  $WHSV = 20 \text{ g}_{\text{syngas}} \text{ min}^{-1} \text{ kg}_{\text{cat}}^{-1}$ ).

Heat transfer resistance of the bed ( $d_R/8\lambda_{er}$ ) rises with the tube diameter whereas heat transfer resistance of the internal reactor ( $1/\alpha_{w,int}$ ) wall remains nearly constant (Fig. 6). Moreover as expected the heat transfer resistance of the wall by conduction is negligible and closed to  $1 \times 10^{-4} \text{ m}^2 \text{ W}^{-1} \text{ K}^{-1}$ . This ability to remove heat released changes so much that not only hot-spot appears but also as WHSV rises heat removal becomes too low to avoid temperature runaway.

Moreover it is particularly interesting to estimate the overall heat transfer coefficient  $U_{overall}$  defined with the assumption that the

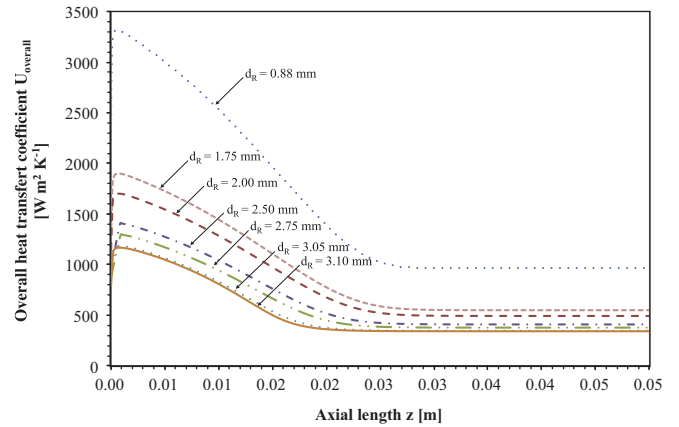


Fig. 7. Overall heat transfer coefficient along axial length for different tube diameters ( $T_w = 493.15 \text{ K}$ ,  $WHSV = 20 \text{ g}_{\text{syngas}} \text{ min}^{-1} \text{ kg}_{\text{cat}}^{-1}$ ).

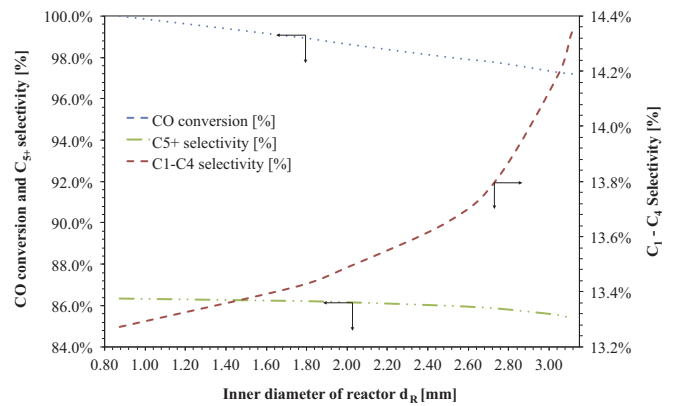


Fig. 8. Effect of tube diameter on CO conversion with  $T_w = 493.15 \text{ K}$ ,  $P = 20 \text{ bar}$  and  $WHSV = 20 \text{ g}_{\text{syngas}} \text{ min}^{-1} \text{ kg}_{\text{cat}}^{-1}$ .

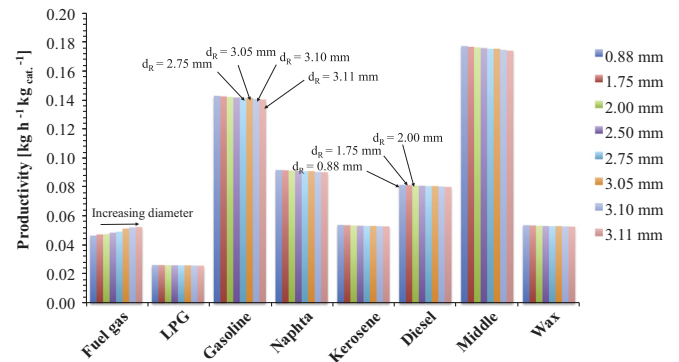


Fig. 9. Effect of tube diameter on productivity of common hydrocarbon cut (fuel gas, liquid petroleum gas (LPG), gasoline, naphtha, jet fuel, diesel, middle distillate, wax) with  $T_w = 493.15 \text{ K}$ ,  $P = 20 \text{ bar}$  and  $WHSV = 20 \text{ g}_{\text{syngas}} \text{ min}^{-1} \text{ kg}_{\text{cat}}^{-1}$ .

external heat transfer resistance of the shell side is negligible due the high flow velocity of the coolant. Therefore, the overall heat transfer coefficient can be written as

$$U_{overall} = \left( \frac{1}{\alpha_{w,int}} + \frac{d_R}{8\lambda_{er}} \right)^{-1} \quad (44)$$

For centimeter tube diameters the calculated overall heat transfer coefficients usually range from around  $200\text{--}400 \text{ W m}^{-2} \text{ K}^{-1}$  (Philippe et al., 2009; Jess and Kern, 2012; Lee and Chung, 2012).

In this work, the overall heat transfer coefficients calculated are much higher (Fig. 7). The coefficient even reaches  $3300 \text{ W m}^{-2} \text{ K}^{-1}$  at the vicinity of the reactor inlet for a 0.88 mm tube diameter. This study reveals also the significant variation of the overall heat transfer along the axial direction  $z$  of the reactor. The value of the gas mixture thermal conductivity strongly associated to the thermal conductivity of hydrogen, increases in the heating zone involving the rise of the overall heat transfer coefficient. As the synthesis starts, the gas mixture conductivity of gas decreases drastically from 132 to  $39 \text{ mW m}^{-1} \text{ K}^{-1}$  due to the consumption of hydrogen and the decrease of gas velocity.

The effect of tube diameter on the conversion of carbon monoxide and the product selectivity is given by Fig. 8. It can be seen that  $C_1$ – $C_4$  fraction increases due to the temperature increases. CO conversion and  $C_{5+}$  selectivity slightly decreases with increasing of tube diameter.

The productivities of hydrocarbon cuts are computed from the recursive kinetics and are shown in Fig. 9. The productivities in liquid transportation fuels (gasoline, Diesel, jet fuel) are found to be slightly affected by the tube diameter while the quantity in fuel gas increases drastically when the tube diameter is increased.

#### 5.4. Influence of WHSV on product selectivity and productivity at constant tube diameter

The influence of space velocity on CO conversion, selectivities and hydrocarbon productivities are presented for two tube diameters:  $d_R = 0.88 \text{ mm}$  (Fig. 10) and  $d_R = 2.75 \text{ mm}$  (Fig. 11). These figures do not exhibit sensitive differences except the  $C_{5+}$  production. Regarding the 0.88 millimeter tube it can be observed that, up to a WHSV of  $80 \text{ g}_{\text{syngas}} \text{ min}^{-1} \text{ kg}_{\text{cat}}^{-1}$ , CO conversion remains approximately constant ( $X_{\text{CO}} = 92\%$ ) whereas the  $C_{5+}$  productivity, which is the total mass flow rate of  $C_{5+}$  hydrocarbons based on catalyst weight, increases and then remains slightly unchanged ( $P_{m_{C_{5+}}} = 2.0 \text{ kg h}^{-1} \text{ kg}_{\text{cat}}^{-1}$ ). Then, as soon as the space velocity reaches values higher than  $90 \text{ g}_{\text{syngas}} \text{ min}^{-1} \text{ kg}_{\text{cat}}^{-1}$ , the conversion decreases and the productivity remains constant ( $P_{m_{C_{5+}}} = 2.0 \text{ kg h}^{-1} \text{ kg}_{\text{cat}}^{-1}$ ) because the residence time decreases below the time needed to convert efficiently the syngas into hydrocarbons. As regards the 2.75 mm tube (Fig. 11) selectivity of  $C_{5+}$  decreases and CO conversion remains both roughly constant up to a space velocity of  $100 \text{ g}_{\text{syngas}} \text{ min}^{-1} \text{ kg}_{\text{cat}}^{-1}$ . Although the  $C_{5+}$  production is higher than within a 0.88 mm tube, an optimal value of space velocity, around  $180 \text{ g}_{\text{syngas}} \text{ min}^{-1} \text{ kg}_{\text{cat}}^{-1}$ , is needed to ensure the maximal production of  $C_{5+}$ . Productivity values of  $C_{5+}$  are in agreement with Sadeqzadeh et al. (2012) for millimeter-scale tubes and the production of light hydrocarbons increases with the rise in tube diameters. Moreover, both Figs. 11 and 10 highlight the weak

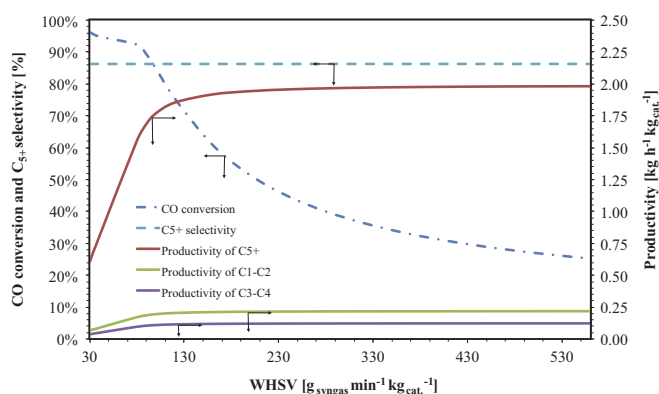


Fig. 10. CO conversion and hydrocarbon productivity versus space velocity WHSV for a millimeter-scale tube  $d_R = 0.88 \text{ mm}$ ,  $T_w = 493.15 \text{ K}$ .

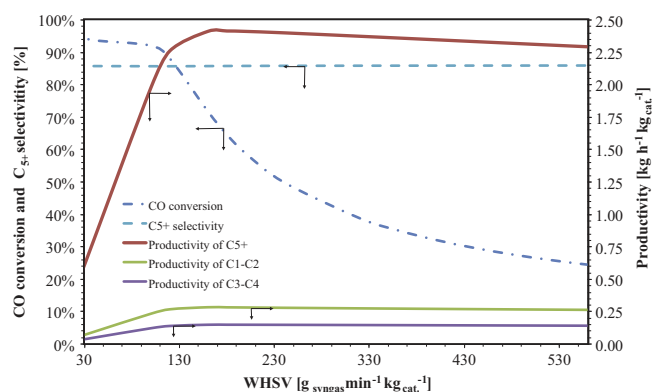


Fig. 11. CO conversion and hydrocarbon productivity versus space velocity WHSV for a centimeter-scale tube  $d_R = 2.75 \text{ mm}$ ,  $T_w = 493.15 \text{ K}$ .

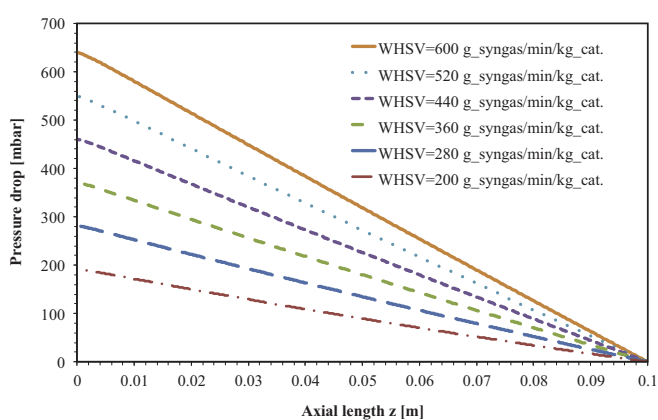


Fig. 12. Pressure drop versus space velocity WHSV for a tube diameter  $d_R = 2.75 \text{ mm}$ ,  $T_w = 493.15 \text{ K}$ .

influence of WHSV on selectivity in  $C_{5+}$ . Actually, a slight increase in temperature around 503 K occurs with 2.75 mm tube and overall heat transfer coefficient is not much dependent on WHSV. High efficiency in heat transfer allows the release of reaction energy and thus prevents the enhancement of light hydrocarbons production.

#### 5.5. Scale-up considerations

Scale-up calculations via numbering-up of tubes were carried out on the basis of the requirement for a production expressed in barrels per day (bpd) of  $C_{5+}$  fraction. Because of the low temperature rise within millimeter-scale geometry, a 2.75 mm tube was chosen. Moreover  $C_{5+}$  selectivity remains higher than 83% whatever the space velocity (Fig. 10) due to the high thermal performance to dissipate heat released. Pressure drops given by simulations for different space velocities as shown in Fig. 12 are strictly linear and obey to an analogous Darcy's law for porous media owing to laminar flow regime because Reynolds number based on particle diameter ( $Re_p$ ) was in the range 0.04–1.

For a 2.75 mm diameter, the scale-up study consist in determining the number of tubes needed to produce one barrel of liquid hydrocarbons ( $N_{\text{tubes}}$ ). According to Table 7, an optimal production of  $2943 \text{ kg h}^{-1} \text{ m}_{\text{cat}}^{-3}$  is ranging around about  $180$ – $200 \text{ g}_{\text{syngas}} \text{ min}^{-1} \text{ kg}_{\text{cat}}^{-1}$  whereas with conventional reactors (fixed bed or slurry), the catalyst productivity of liquid hydrocarbons does not exceed  $400 \text{ kg h}^{-1} \text{ m}_{\text{cat}}^{-3}$  (Oxford Catalyst, 2012). This range of value is in agreement with the microreactor used by Velocys (Deshmukh et al., 2010).

**Table 7**  
Results for the scale-up calculations for a 2.75 mm tube diameter,  $T_w = 493.15$  K.

WHSV ( $\text{g}_{\text{syngas}} \text{min}^{-1} \text{kg}_{\text{cat}}^{-1}$ )	$u_{s,0}$ ( $\text{mm s}^{-1}$ )	$X_{\text{CO}}$ (%)	$S_{\text{C}_{5+}}$ (%)	$P_{\text{C}_{5+}}$ ( $\text{kg h}^{-1} \text{m}_{\text{cat}}^{-3}$ )	$N_{\text{tubes}}$ (tubes bpd $^{-1}$ )
20	4.64	97.73	85.80	510.6	17484
30	6.96	94.54	85.80	741.3	12 042
40	9.28	93.70	85.78	979.9	9111
100	23.19	92.08	85.73	2409.2	3706
160	37.11	71.80	85.77	2939.7	3037
180	41.75	64.65	85.80	2943.3	3033
200	46.38	58.79	85.83	2939.4	3037
240	55.66	49.94	85.86	2926.0	3051
320	74.21	38.82	85.89	2893.7	3085
360	83.49	35.11	85.90	2877.3	3103
400	92.28	32.14	85.91	2860.8	3121
440	102.05	29.71	85.92	2844.2	3139
560	129.88	24.51	85.95	2794.8	3194
600	139.15	23.23	85.96	2778.6	3213

## 6. Conclusions

Simulation results based on the described two dimensional model have shown a high dependency of the thermal behavior with respect to the thermal conductivity of the gas mixture, which is linked to the hydrogen consumption, exhibiting a high thermal conductivity compared with other compounds, along the reactor. Although the viscosity and the heat capacity slightly change during synthesis, this variation does not cause the same variation of temperature within the bed. The simulations of different tube diameters of the fixed-bed reactor allowed to highlight the high performance of millimeter-scale for FT synthesis. No exact convergence was achieved for diameter tube higher than 3.11 mm due to the thermal runaway affecting the other variables strongly coupled. Therefore, in the work reported here using a kinetic associated with a highly active catalyst, the critical diameter involving a hot spot lower than 10 K is found to be lower 2.50 mm. No significant temperature rise occurs below this diameter range preventing the increase of light hydrocarbons selectivity. Millichannel catalytic reactor provides effective heat removal for this exothermic synthesis, leading to an isothermal temperature profile which induces low methane selectivity and production of long chain hydrocarbons. The campaign of simulations also allowed to find out an optimal space velocity to maximize the production rate of  $\text{C}_{5+}$ . Results obtained from scale-up study open a promising way to produce more hydrocarbons with compact module unit where temperature becomes a controllable parameter.

## Nomenclature

### Greek letters

$\alpha$	chain growth probability (dimensionless)
$\alpha_{w,int}$	wall heat transfer coefficient ( $\text{W m}^{-2} \text{K}^{-1}$ )
$\beta_F$	Forchheimer coefficient ( $\text{m}^{-1}$ )
$\Delta H_{f,i}$	enthalpy of formation of specie $i$ ( $\text{J mol}^{-1}$ )
$\Delta H_R$	global heat of reaction of FT synthesis ( $\text{J mol}_{\text{CO}}^{-1}$ )
$\epsilon$	bed void fraction (dimensionless)
$\epsilon_p$	catalyst permeability (dimensionless)
$\eta$	effectiveness factor (dimensionless)
$\lambda_{bed}$	bed thermal conductivity ( $\text{W m}^{-1} \text{K}^{-1}$ )
$\lambda_{ea}$	effective axial thermal conductivity ( $\text{W m}^{-1} \text{K}^{-1}$ )
$\lambda_{er}$	effective radial thermal conductivity ( $\text{W m}^{-1} \text{K}^{-1}$ )
$\lambda_{g,i}$	thermal conductivity of gaseous specie $i$ ( $\text{W m}^{-1} \text{K}^{-1}$ )

$\lambda_{g,m}$	thermal conductivity of gas mixture ( $\text{W m}^{-1} \text{K}^{-1}$ )
$\lambda_{wall}$	thermal conductivity of the wall ( $\text{W m}^{-1} \text{K}^{-1}$ )
$\mu_{g,i}$	viscosity of gaseous specie $i$ (Pa s)
$\mu_{g,m}$	viscosity of gas mixture (Pa s)
$\phi$	Thiele's modulus (dimensionless)
$\rho_f$	density of gas mixture ( $\text{kg m}^{-3}$ )
$\rho_p$	density of particle catalyst ( $\text{kg m}^{-3}$ )
$\tau_p$	tortuosity (dimensionless)
$\theta_{\text{H}_2/\text{CO}}$	molar ratio $\text{H}_2/\text{CO}$ (dimensionless)

### Latin letters

$\vec{J}_i$	mass diffusional flux for the specie $i$ ( $\text{kg m}^{-2} \text{s}^{-1}$ )
$\vec{u}$	velocity profile ( $\text{m s}^{-1}$ )
$a$	pre-exponential factor in Arrhenius' law ( $\text{m}^6 \text{kg}_{\text{cat}}^{-1} \text{mol}^{-1} \text{s}^{-1}$ )
$b$	pre-exponential factor in Arrhenius' law ( $\text{m}^3 \text{mol}^{-1}$ )
$C_i$	molar concentration of specie $i$ ( $\text{mol m}^{-3}$ )
$d$	pre-exponential factor in Arrhenius' law (dimensionless)
$d_p$	pellet diameter (m)
$d_R$	inner tube diameter (m)
$D_{ea}$	effective axial dispersion coefficient ( $\text{m}^2 \text{s}^{-1}$ )
$D_{\text{eff},\text{H}_2,i}$	effective diffusion coefficient of hydrogen ( $\text{m}^2 \text{s}^{-1}$ )
$D_{er}$	effective radial dispersion coefficient ( $\text{m}^2 \text{s}^{-1}$ )
$e$	pre-exponential factor in Arrhenius' law (dimensionless)
$F$	inlet mass flow ( $\text{kg s}^{-1}$ )
$He_{\text{H}_2}$	Henry's coefficient ( $\text{Pa m}^3 \text{mol}^{-1}$ )
$I$	identity matrix (-)
$K$	porous media permeability ( $\text{m}^2$ )
$k'_a$	apparent constant rate of consumption of CO ( $\text{m}^3 \text{kg}_{\text{cat}}^{-1} \text{s}^{-1}$ )
$k_a$	constant rate of consumption of CO ( $\text{m}^6 \text{kg}_{\text{cat}}^{-1} \text{mol}^{-1} \text{s}^{-1}$ )
$k_b$	adsorption constant ( $\text{m}^3 \text{mol}^{-1}$ )
$k_{FT}$	kinetic constant of FT synthesis ( $\text{m}^6 \text{kg}_{\text{cat}}^{-1} \text{mol}^{-1} \text{s}^{-1}$ )
$L$	length of reactor (m)
$m$	mass (kg)
$N$	chain number of hydrocarbons (dimensionless)
$N_{\text{tubes}}$	number of tubes needed to produce one barrel of liquid hydrocarbons ( $\text{C}_{5+}$ ) per day (tubes bpd $^{-1}$ )
$P_i$	partial pressure of specie $i$ (Pa)
$P_{\text{C}_{5+}}$	mass production of ( $\text{kg h}^{-1} \text{m}_{\text{cat}}^{-3}$ )
$P_{out}$	outlet pressure (Pa)
$r$	radial length (m)
$r_i$	rate of consumption of specie $i$ ( $\text{mol s}^{-1} \text{kg}_{\text{cat}}^{-1}$ )
$r_{\text{CO,effective}}$	global reaction rate of CO consumption $i$ ( $\text{mol s}^{-1} \text{kg}_{\text{cat}}^{-1}$ )
$r_{\text{CO,surface}}$	intrinsic reaction rate of CO consumption $i$ ( $\text{mol s}^{-1} \text{kg}_{\text{cat}}^{-1}$ )
$Re_p$	Reynolds number (dimensionless)
$S$	selectivity (dimensionless)
$T$	bulk temperature (K)
$T_0$	inlet temperature (K)
$T_w$	cooling temperature (K)
$u_z$	axial velocity profile ( $\text{m s}^{-1}$ )
$U_{\text{overall}}$	overall thermal transmittance ( $\text{W m}^{-2} \text{K}^{-1}$ )
$u_{s,0}$	inlet velocity ( $\text{m s}^{-1}$ )
$u_{wall}$	velocity near the wall vicinity ( $\text{m s}^{-1}$ )
$w_i$	mass fraction of specie $i$ (dimensionless)
WHSV	weight hourly space velocity ( $\text{g}_{\text{syngas}} \text{min}^{-1} \text{kg}_{\text{cat}}^{-1}$ )
$X_{\text{CO}}$	CO conversion (dimensionless)

$z$  axial direction (m)  
 $c_{p,g,m}$  heat capacity of the specie  $i$  ( $\text{J kg}^{-1} \text{K}^{-1}$ )

## Acknowledgments

The authors are grateful to Pr. Fongarland Pascal, University Claude-Bernard Lyon 1, IRCELYon, for the helpful discussions concerning Fischer-Tropsch synthesis.

## References

- Anderson, R.B., Friedel, R.A., Storch, H.H., 1951. Fischer-Tropsch reaction mechanism involving stepwise growth of carbon chain. *J. Chem. Phys.* 19, 313–319.
- Atwood, H.E., Bennett, C.O., 1979. Kinetics of the Fischer-Tropsch reaction over iron. *Ind. Eng. Chem. Process Des. Dev.* 18, 163–170.
- Bauer, R., Schlunder, E., 1978a. Effective radial thermal conductivity of packing in gas flow. Part I. convective transport coefficient. *Int. Chem. Eng.* 18, 181–188.
- Bauer, R., Schlunder, E., 1978b. Effective radial thermal conductivity of packing in gas flow. Part II. Thermal conductivity of the packing fraction without gas flow. *Int. Chem. Eng.* 18, 181–188.
- Borkink, J.G.H., Westerterp, K.R., 1992. Influence of tube and particle diameter on heat transport in packed beds. *AIChE J* 38, 703–715.
- Brokaw, R.S., 1969. Predicting transport properties of dilute gases. *Ind. Eng. Chem. Process Des. Dev.* 8, 240–253.
- Bub, G., Baerns, M., Büssemeier, B., Frohning, C., 1980. Prediction of the performance of catalytic fixed bed reactors for Fischer-Tropsch synthesis. *Chem. Eng. Sci.* 35, 348–355.
- Cao, C., Hu, J., Li, S., Wilcox, W., Wang, Y., 2009. Intensified Fischer-Tropsch synthesis process with microchannel catalytic reactors. *Catal. Today* 140, 149–156.
- Chambrey, S., Fongarland, P., Karaca, H., Piché, S., Griboval-Constant, A., Schweich, D., Luck, F., Savin, S., Khodakov, A.Y., 2011. Fischer-Tropsch synthesis in milli-fixed bed reactor: comparison with centimetric fixed bed and slurry stirred tank reactors. *Catal. Today* 171, 201–206.
- Chukwudozie, C.P., Tyagi, M., Sears, S.O., White, C.D., 2012. Prediction of non-Darcy coefficients for inertial flows through the castlegate sandstone using image-based modeling. *Transp. Porous Med.* 95, 563–580.
- Delgado, J.M.P.Q., 2006. A critical review of dispersion in packed beds. *Heat Mass Transfer* 42, 279–310.
- Deshmukh, S.R., Tonkovich, A.L.Y., Jarosch, K.T., Schrader, L., Fitzgerald, S.P., Kilanowski, D.R., Lerou, J.J., Mazanec, T.J., 2010. Scale-up of microchannel reactors for Fischer-Tropsch synthesis. *Ind. Eng. Chem. Res.* 49, 10883–10888.
- Dry, M.E., 2002. The Fischer-Tropsch process: 1950–2000. *Catal. Today* 71, 227–241.
- Fuller, E.N., Ensley, K., Giddings, J.C., 1969. *J. Phys. Chem.* 73.
- Fuller, E.N., Giddings, J.C., 1965. *J. Gas Chromatogr.* 3.
- Fuller, E.N., Schettler, P.D., Giddings, J.C., 1966. *Ind. Eng. Chem.* 58.
- Guillou, L., 2005. Synthèse de Fischer-Tropsch en réacteurs structurés à catalyse supportée en paroi (Ph.D. thesis), Ecole Centrale Lille.
- Huff, G.A., Satterfield, C.N., 1984. Intrinsic kinetics of the Fischer-Tropsch synthesis on a reduced fused-magnetite catalyst. *Ind. Eng. Chem. Process Des. Dev.* 23, 696–705.
- Jess, A., Kern, C., 2009. Modeling of multi-tubular reactors for Fischer-Tropsch synthesis. *Chem. Eng. Technol.* 32, 1164–1175.
- Jess, A., Kern, C., 2012. Influence of particle size and single-tube diameter on thermal behavior of Fischer-Tropsch reactors. Part I. Particle size variation for constant tube size and vice versa. *Chem. Eng. Technol.* 35, 369–378.
- Jess, A., Popp, R., Hedden, K., 1999. Fischer-Tropsch-synthesis with nitrogen-rich syngas: fundamentals and reactor design aspects. *Appl. Catal. A: General* 186, 321–342.
- Khodakov, A.Y., Chu, W., Fongarland, P., 2007. Advances in the development of novel cobalt Fischer-Tropsch catalysts for synthesis of long-chain hydrocarbons and clean fuels. *Chem. Rev.* 107, 1692–1744.
- Knochen, J., Güttel, R., Knobloch, C., Turek, T., 2010. Fischer-Tropsch synthesis in milli-structured fixed-bed reactors: experimental study and scale-up considerations. *Chem. Eng. Process.: Process Intensif.* 49, 958–964.
- Lee, T.S., Chung, J.N., 2012. Mathematical modeling and numerical simulation of a Fischer-Tropsch packed bed reactor and its thermal management for liquid hydrocarbon fuel production using biomass syngas. *Energy Fuels* 26, 1363–1379.
- Marpu, D.R., 1995. Forchheimer and Brinkman extended Darcy flow model on natural convection in a vertical cylindrical porous annulus. *Acta Mech.* 109, 41–48.
- Martin, H., Nilles, M., 1993. Radiale Wärmeleitung in durchströmten Schüttungsrohren. *Chem. Ing. Tech.* 65, 1468–1477.
- Myrstad, R., Eri, S., Pfeifer, P., Rytter, E., Holmen, A., 2009. Fischer-Tropsch synthesis in a microstructured reactor. *Catal. Today* 147 (Supplement), S301–S304.
- National Institute of Standards and Technology (NIST), 2013. Available on (<http://webbook.nist.gov/chemistry/liquid/>). Consulted September 9, 2013.
- Newsome, D.S., 1980. The water-gas shift reaction. *Catal. Rev.* 21, 275–318.
- Nield, D.A., Bejan, A., 2013. *Convection in Porous Media*. Springer, New York.
- Outi, A., Rautavuoma, I., van der Baan, H.S., 1981. Kinetics and mechanism of the Fischer Tropsch hydrocarbon synthesis on a cobalt on alumina catalyst. *Appl. Catal.* 1, 247–272.
- Oxford Catalyst, 2012. Available on (<http://www.velocys.com>), Consulted December 16, 2013.
- Özgümiş, T., Mobedi, M., Özkol, U., Nakayama, A., 2013. Thermal dispersion in porous media—a review on the experimental studies for packed beds. *Appl. Mech. Rev.* 65, 031001.
- Philippe, R., Lacroix, M., Dreibine, L., Pham-Huu, C., Edouard, D., Savin, S., Luck, F., Schweich, D., 2009. Effect of structure and thermal properties of a Fischer-Tropsch catalyst in a fixed bed. *Catal. Today* 147 (Supplement), S305–S312.
- Poling, B., Prausnitz, J., Connell, J.O., 2000. *The Properties of Gases and Liquids*. McGraw Hill, New York.
- Sadeqzadeh, M., Hong, J., Fongarland, P., Curulla-Ferré, D., Luck, F., Bousquet, J., Schweich, D., Khodakov, A.Y., 2012. Mechanistic modeling of cobalt based catalyst sintering in a fixed bed reactor under different conditions of Fischer-Tropsch synthesis. *Ind. Eng. Chem. Res.* 51, 11955–11964.
- Sarup, B., Wojciechowski, B.W., 1989. Studies of the Fischer-Tropsch synthesis on a cobalt catalyst II. Kinetics of carbon monoxide conversion to methane and to higher hydrocarbons. *Can. J. Chem. Eng.* 67, 62–74.
- Springer (Ed.), 2010. *VDI Heat Atlas*. VDI-Gesellschaft Verfahrenstechnik und Chemieingenieurwesen, second edition. VDI Gesellschaft.
- Wang, Y.N., Xu, Y.Y., Li, Y.W., Zhao, Y.L., Zhang, B.J., 2003. Heterogeneous modeling for fixed-bed Fischer-Tropsch synthesis: reactor model and its applications. *Chem. Eng. Sci.* 58, 867–875.
- Wu, J., Zhang, H., Ying, W., Fang, D., 2010. Simulation and analysis of a tubular fixed-bed Fischer-Tropsch synthesis reactor with co-based catalyst. *Chem. Eng. Technol.* 33, 1083–1092.
- Yates, I.C., Satterfield, C.N., 1991. Intrinsic kinetics of the Fischer-Tropsch synthesis on a cobalt catalyst. *Energy Fuels* 5, 168–173.
- Yaws, C., 1999. *Chemical Properties Handbook: Physical, Thermodynamics, Environmental Transport, Safety & Health Related Properties for Organic and Inorganic Chemicals*. McGraw-Hill Education, New York.
- Zimmerman, W.H., Bukur, D.B., 1990. Reaction kinetics over iron catalysts used for the Fischer-Tropsch synthesis. *Can. J. Chem. Eng.* 68, 292–301.